The Mapping of the Plasma Sheath in a Magnetic Field

Hannah Sabo, Michael Dropmann, Rene Laufer, and Truell Hyde

***Abstract*—The interaction between plasma and a static magnetic field is investigated experimentally. A cylindrical dipole magnet was placed in horizontal orientation underneath a glass surface and placed into a Gaseous Electronics Conference Radio Frequency Reference Cell. Experiments were run with the magnet dipole axis oriented both parallel and perpendicular to the camera axis. Experiments were conducted at a pressure of 1.33 and 5.33 Pa and melamine formaldehyde particles were introduced into plasma, acting as a diagnostic tool and reacting to the forces in the plasma. The electric accelerations in both the vertical and horizontal directions are a result of the presence of the magnetic field. It was found that these vertical and horizontal forces caused confinement, resulting in complex motion and horizontal transport of the dust particles within the plasma.**

***Index Terms*—Dusty plasmas, Magnetic confinement, Moon, Plasma sheath**

I. Introduction

ALTHOUGH appearing very different, the Earth and the Moon have an almost identical composition of materials. The titanium and oxygen isotopic compositions were found to be identical but quite rare compared to other materials in the universe [1], [2]. Still, the Moon and the Earth are quite different. Unlike the Earth, the Moon lacks both an atmosphere and a global magnetic field. The solar wind, a space plasma, impacts the surface of the Moon and weathers the lunar regolith, causing it to age and turn to a darker color than it previously was.

On the Moon, there are some large swirls of lighter albedo than its surroundings. This might indicate that the soil over those particular regions have aged less than the regolith surrounding these patches. This implies that the lunar swirl regions might have been more shielded from the solar wind than the regions surrounding it [3]. These lunar swirls, such as the Reiner Gamma Formation, appear to be independent of any topographical features, such as mountains, valleys, and craters [3]. However, the swirls on the surface of the Moon correspond to areas of significant localized magnetic fields. Magnetometer and electron reflectometer data from Lunar Prospector have shown that these magnetic fields are found to range in size from approximately 4 km to a couple hundred kilometers and range in strength from very weak to 100 nT [4]. So, there is a connection between the areas on the moon with a higher lunar albedo and these magnetic anomalies. Low orbiting space probes determined there to be a low density ion cavity above these lunar regions that is about the same size as the magnetic field [3].

It is likely that this bubble is created from the interaction between the solar wind and the localized magnetic field. As the positive ions and negative electrons in the solar wind encounter a magnetic field as they approach the lunar surface. The Larmor radius is

$$r_g = \frac{mv_\perp}{|q|B} \qquad (1)$$

So, due to the light mass of an electron, the Larmor radius is much smaller than that of a proton. In fact, compared to the size of a magnetic lunar anomaly, the ions in the solar wind do not gyrate at all. However, the electrons do. Therefore, in the stream, the electrons are considered magnetized and ions are not. The ions are thus not affected directly by the magnetic field, while the magnetized electrons are deflected by the magnetic field. This leads to a separation of charges that can create strong electric fields capable of reflecting ions.

The interaction of plasmas and magnetic fields is an area of interest for many areas of research. There have been recent efforts to create lunar swirl environments in the lab [3], [5], [6].

The experiments presented in this paper serve as precursor experiments to experiments in a streaming plasma that are planned to be conducted in the inductively heated plasma generator IPG6-B.

II. Methods

A. Materials and Procedure

Dusty or complex plasmas are mixtures of ionized gases and charged particles. In the lab, the dust particles are suspended in

Manuscript received August 5, 2014. This work was supported in part by the National Science Foundation.

H. C. Sabo is with CASPER, Baylor University, Waco, TX 76798 USA. She is an undergraduate student at Seattle Pacific University, (e-mail: saboh@spu.edu).
M. Dropmann is with CASPER, Baylor University, Waco, TX 76798 USA (e-mail: michael_dropmann@baylor.edu) as well as with the University of Stuttgart, Stuttgart, Germany
R. Laufer was with the University of Stuttgart, Stuttgart, Germany. He is now with CASPER, Baylor University, Waco, TX 76798 USA (e-mail: rene_laufer@baylor.edu).
T. W.Hyde is with CASPER, Baylor University, Waco, TX 76798 USA (e-mail: truell_hyde@baylor.edu).

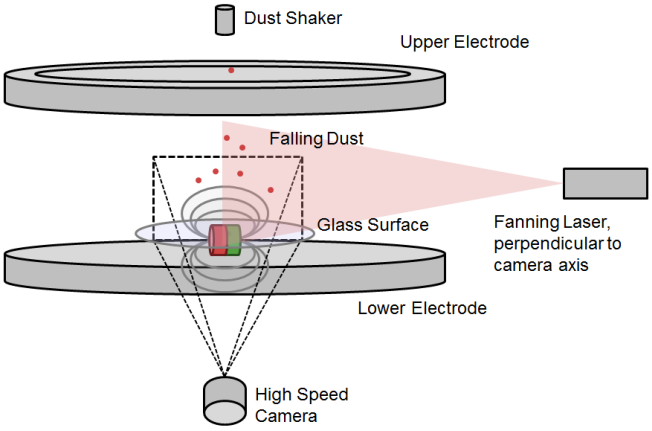

Fig. 1. The experiment setup in the GEC RFreference cell. A horizontally oriented magnet within a glass and Teflon (PTFE) table is placed on the lower electrode. Dust is sprinkled in from a dropper above the upper electrode. The dust is illuminated by a vertical fanning laser oriented perpendicular to the camera.

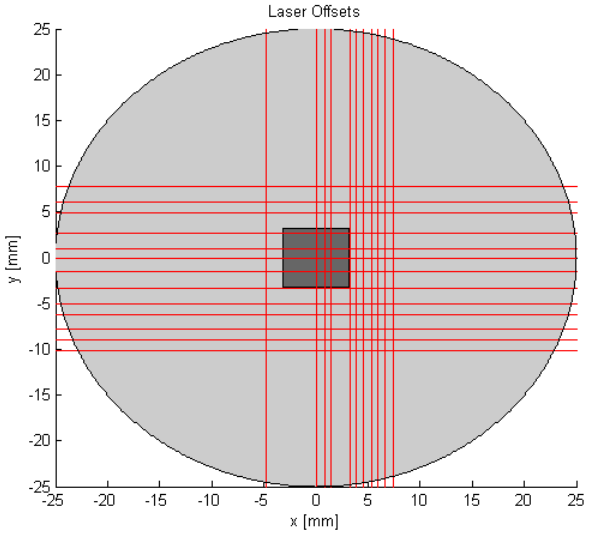

Fig. 2. A top view of the GEC RF reference cell. The dark gray box in the center shows the position of the magnet, while the light gray circle represents the glass surface. The red lines indicate the different positions of the laser. In order to get a 3D sense of the forces in the magnetically confined plasma, data was not only taken along the center, but at several data offsets, called slices. Slices were taken when the magnet was positioned both parallel and perpendicular to the camera axis. In this image, the magnet dipole is oriented horizontally.

plasma and acquire a negative charge due to impacts with the fast-moving electrons [7]. In these experiments, dusty plasma is not used as analog for the lunar regolith, but rather serves as a diagnostic tool. The dust functions as a probe by gaining a charge and interacting with the electric fields within the plasma.

These experiments serve as precursor experiments to the study of lunar swirls and the interactions between lunar magnetic anomalies and the solar wind, rather than replicate the exact lunar environment. However, these experiments attempt to replicate parameters of lunar swirls. The proportional size of the Larmor radius of protons and electrons to the size of the dust swirl was consistent in the experiments.

The experiments were conducted in a Gaseous Electronics Conference radio frequency reference cell, which reliably replicates plasma conditions from day to day and laboratory to laboratory [8]. Shown in Fig. 1, a 5 cm Teflon (PTFE) table with a glass surface was set on the lower electrode. Like the lunar soil, glass can be charged and retain that charge, but is nonconductive. So it was chosen for these experiments. In the center of the Teflon table, under the glass, a cylindrical NeFeB magnet of 6.35 mm diameter and length with a magnetic strength of 1.24-1.28 T was placed in a horizontal orientation. Argon gas was added to the cell and ignited into a plasma with radio frequency waves. 12 micrometer melamine formaldehyde (MF) dust particles were dropped into the plasma via a dust shaker. These gained a negative charge and acted as a probe, as they were affected by the electric forces in the plasma. From the outside of the chamber, a vertical fanning laser with a wavelength of 660 nm was oriented perpendicular to the view of a high speed camera. The laser illuminated the dust particles in the field of view of the camera.

For the first set of experiments, the dipole axis of the magnet was oriented parallel to the high speed camera axis. The plasma pressure was set to 5.33 Pa (40 mTorr) and the RF power was set to 11.3 W. The high speed camera took data at 2000 frames per second. A random amount of dust particles were dropped from the dust shaker into the plasma for each data run. As they fell through the plasma, they were bombarded by electrons, which have a relatively high speed compared to the heavier ions, and acquired a negative charge. This charge caused the particles to be susceptible to electric forces, which significantly affected the trajectories of the particle. The laser initially started out centered over the magnet. In order to generate a 3D data-set the laser was moved to different offsets in respect to the center during the course of experiments. Each position can be seen in Fig. 2. Following this set of experiments, the magnet was reoriented so that the magnet's dipole axis was perpendicular to the high speed camera. The procedure was then repeated. Ultimately, data was taken at 12 laser positions when the magnet was oriented parallel to the camera and 13 when it was oriented perpendicular to the camera.

In another set of experiments, the setup still remained as it is in Fig. 1. However, the valve that delivers argon from the canister to the GEC was closed. The pressure slowly dropped to 1.33 Pa (10 mTorr). As the needle valve, which controls the argon, cannot be set to a value low enough to stably maintain 1.33 Pa, the main argon valve was closed. While the pressure dropped, the RF power increased. So, prior to shutting off the argon, it needed to be adjusted so that when the pressure reached 1.33 Pa, the radio frequency was at 11.3 Watts, similar to conditions of the 5.3 Pa experiments. At this moment, the particles were dropped from the dust shaker, and the data was recorded. Immediately following the data collection, the argon valve was reopened, and the initial conditions returned. Data was taken with the magnet dipole axis both parallel and perpendicular to the high speed camera. The data from the low pressure experiments was analyzed using the same procedure as the 5.33 Pa experiments.

For both the 5.33 Pa and the 1.33 Pa experiments, reference experiments were taken. The magnet was removed from the setup and the glass table remained. The procedure was followed as before. These measurements allowed the influences of the magnet and the table to be seen separately and is a good experiment to reference when considering data.

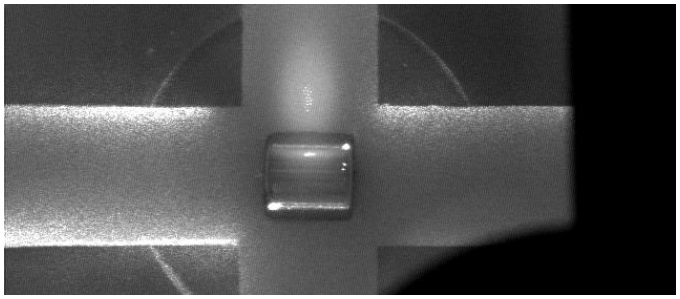

Fig. 3. A top view into the GEC RF reference cell. When the magnet was oriented horizontally, a bright spot or bulge appeared in the plasma and can be seen in this figure above the magnet. As seen the in image, this bright spot was an area of stable particle levitation.

B. Analysis Methods

The high speed camera image sequences from the lab were imported to ImageJ, an image processing and analyzing program. Functions from the MosaicSuite plugin were used. Using the MosaicSuite, the background was subtracted from the images to remove the background noise. Then the brightness and contrast was adjusted to make the particles and their paths clearer. MATLAB was then used to locate the particles in each frame and link together trajectories of the same particle.

The trajectories were smoothed, and from these the positions, velocities, and accelerations of the particles in both the horizontal and vertical directions were calculated. All of the data from each frame and trial was merged onto one data set on a standard coordinate system. In this paper the mentioned 3D data will not be shown yet. Only 2D data slices that have a zero offset from the center of the magnet are presented. The data set was broken into a 30 by 110 grid. For each point, a radius of 1 mm around it was taken. Each particle that fell within this radius was considered and was then fit with a linear regression of the acceleration vs. velocity. The rest acceleration, when the velocity was zero, was taken and used to create a map of the acceleration at each location. This was done for the horizontal and vertical directions. Thus, the accelerations and the net forces on particles in the plasma sheath were found and mapped.

III. RESULTS

A. Observations from Experiments

For all of the experiments, the magnet was oriented horizontally in the table. In these experiments, shown in figure 3, a region of the plasma glowed noticeably brighter than the plasma surrounding it. This bulge reliably and repeatedly showed up in all of the experiments to the left of the center of the magnet when the observer faces the south pole. Additionally, this bright spot acted as a stable levitation region for the MF particles.

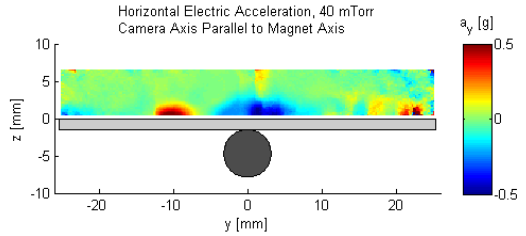

Fig. 4 The setup including a plate (light grey) and magnet oriented parallel to the dipole axis (dark grey circle). The horizontal acceleration when the pressure is set to 5.33 Pa the camera axis is oriented parallel to the magnetic dipole axis, along the x-axis. In this figure, the darkest blue represents an acceleration of ½ g to the left. The darkest red represents an acceleration of ½ g towards the right. The green represents a zero horizontal acceleration.

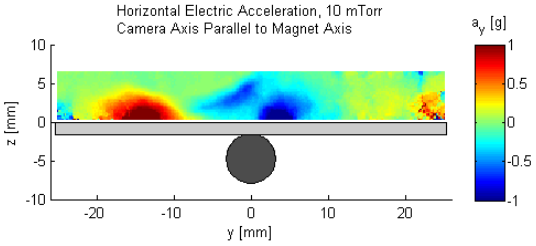

Fig. 5 The setup with the horizontal acceleration when the pressure is set to 1.33 Pa the camera axis is oriented parallel to the magnetic dipole axis, along the x-axis. In this figure, the darkest blue represents an acceleration of 1 g to the left. The darkest red represents an acceleration of 1 g towards the right. The green represents a zero horizontal acceleration.

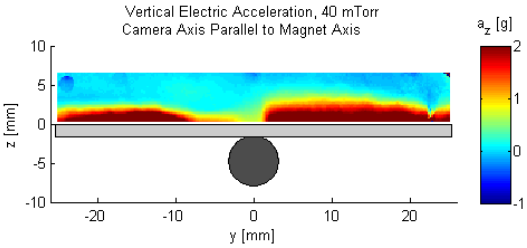

Fig. 6 The setup and the vertical acceleration when the pressure is set to 5.33 Pa the camera axis is oriented parallel to the magnetic dipole axis, along the x-axis. In this figure, the darkest blue represents an acceleration of 1 g down. The darkest red represents an acceleration of 2 g upwards, closest to the glass plate. The cyan represents a zero vertical acceleration.

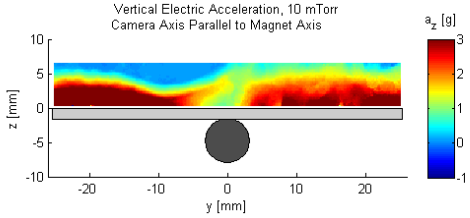

Fig. 7 The setup and the vertical acceleration when the pressure is set to 1.33 Pa the camera axis is oriented parallel to the magnetic dipole axis, along the x-axis. In this figure, the darkest blue represents an acceleration of 1 g down. The darkest red represents an acceleration of 3 g upwards, closest to the glass plate. The cyan represents a zero vertical acceleration

B. Camera Axis Parallel to Magnet Dipole Axis

When the camera was oriented parallel to the magnet dipole axis, maps were produced for both the horizontal acceleration forces and the vertical acceleration forces. When the pressure was at 5.33 Pa, as seen in Fig. 4, the forces are asymmetric at the center. On the left side of the magnet around the -10 mm position, there is a strong push to the right, towards the center

of the magnet. Above the center of the magnet, there is a large area with a strong force pushing particles to the left. Near the ends of the table, there are electric forces off the edge of the table. The left side has accelerations to the left, and the right side to the right. When the pressure was lowered to 1.33 Pa, seen in Fig. 5, the strongest accelerations double from a magnitude of half a g to one g. The areas have both expanded. The region that was at -10 mm has spread to -15 mm. The region with acceleration to the left above the magnet has increased in size and there are now too regions of intense force. However, the accelerations near the edge of the table are unchanged.

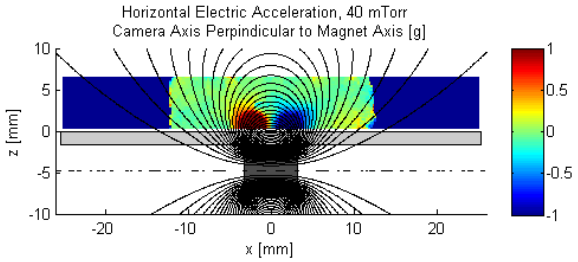

Fig. 8 The setup including a plate (light grey) and magnet oriented perpendicular to the dipole axis (dark grey rectangle). The field lines of the magnet have been plotted in black. The horizontal acceleration when the pressure is set to 5.33 Pa the camera axis is oriented perpendicular to the magnetic dipole axis, along the y-axis. In this figure, the darkest blue on the edges is from a lack of data in that area. There are two spots of strong force, the red area to the left of the center of the magnet represents an acceleration of 1 g to the right, while the blue region represents a strong acceleration of 1 g to the left.

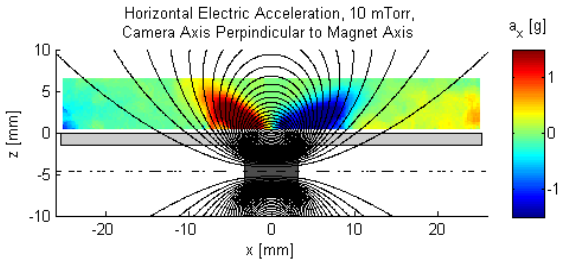

Fig. 9. The setup including a plate (light grey) and magnet oriented perpendicular to the dipole axis (dark grey circle). The horizontal acceleration when the pressure is set to 1.33 Pa the camera axis is oriented perpendicular to the magnetic dipole axis, along the y-axis. In this figure, the darkest blue represents an acceleration of 1.5 g to the left. The darkest red represents an acceleration of 1.5 g towards the right.

Shown in Fig. 6, when the vertical accelerations were calculated for the 5.33 Pa experiments, there were regions of intense upwards acceleration, at least two g, directly above the table. There is a small dip slightly to the left of the magnet where the acceleration upwards is less intense, an acceleration of about one g. When the pressure was dropped from 5.33 Pa to 1.33 Pa, like in Fig. 7, the upward acceleration from the surface of the table increased to at least three g. Directly above the magnet, a pocket of less intense acceleration is almost surrounded by strong accelerations.

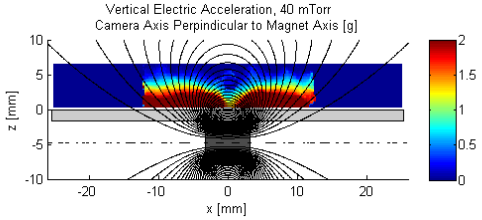

Fig. 10. The setup including a plate (light grey) and magnet oriented perpendicular to the dipole axis (dark grey square). The horizontal acceleration when the pressure is set to 5.33 Pa the camera axis is oriented perpendicular to the magnetic dipole axis, along the y-axis. In this figure, the deepest red of more than 2 g upward. There are dark blue regions on the left and right where there was no data taken.

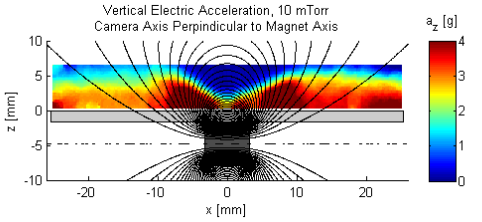

Fig. 11. The setup including a plate (light grey) and magnet oriented perpendicular to the dipole axis (dark grey square). The horizontal acceleration when the pressure is set to 1.33 Pa the camera axis is oriented perpendicular to the magnetic dipole axis, along the y-axis. In this figure, the darkest blue represents an acceleration of 0 g downward. The darkest red represents an acceleration of 4 g upwards.

C. Camera Axis Perpendicular to Magnet Dipole Axis

As seen in Fig. 8, when the camera axis was oriented perpendicular to the magnetic dipole axis and the pressure is set to 5.33 Pa, the horizontal accelerations are symmetric. From the left side of the magnet, there is an acceleration of about 1 g to the center. From the right side, there is a push of 1 g to the left. Directly above the center of the magnet, about where the magnetic field lines are parallel to the surface, the horizontal acceleration is very small. This leads to the effect that the particles are being pushed into the region above the magnet. When the pressure was dropped to 1.33 Pa, shown in Fig. 9, the regions of strong acceleration grew and the magnitude of accelerations in these areas increased. At the edges of the glass table, there are accelerations directed away from the table, similar to the accelerations at the edge of the table when the camera was oriented parallel to the magnetic dipole axis. This is not visible in the 5.33 Pa experiments due to the lack of data in these regions.

When the vertical forces were measured at 5.33 Pa, seen in Fig. 10, there was an acceleration upwards of at least 2 g. This region of intense force was strongest near the edges of the magnet. Like in other experiments, there is a dip in intensity of the vertical acceleration forces above the center of the magnet, where the field lines are parallel to the surface. Similar to the other experiments, when the pressure was at 1.33 Pa, seen in Fig. 11, the intensity of the acceleration increased. There are regions where there is a force of 4 g upwards. The dip above the center of the magnet was again slightly greater than in the 5.33 Pa experiments.

D. Reference Experiments

In addition to experiments with the magnet, data was also taken with an aluminum cylinder in place of the magnet. Seen in Fig. 12, there were forces of less than ½ g towards the edge of the table that was the closest. At the edge of the table, these forces are the most intense. Further the vertical acceleration appears to be weaker at the surface of the table but decreases with a smaller gradient leading to a thicker plasma sheath.

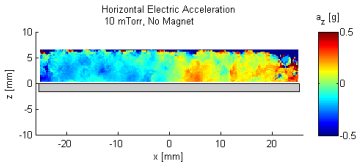

Fig. 12. The setup including a plate (light grey) with no magnet. The horizontal acceleration when the pressure is set to 1.33 Pa. In this figure, the darkest blue represents an acceleration of ½ g left. The darkest red represents an acceleration of ½ g right.

IV. Discussion

When the magnet was oriented horizontally in the GEC RF reference cell, there was a noticeably brighter bulge in the plasma, off the center of the magnet. This bulge was shown in fig. 3. One theory for the emergence of this brighter area is the Lorentz force

$$\boldsymbol{F} = q(\boldsymbol{E} + \boldsymbol{v} \times \boldsymbol{B}) \qquad (3)$$

exerted on the ion flow towards the glass surface.

Another possible reason for the plasma glow was the $\boldsymbol{E} \times \boldsymbol{B}$ drift on the electrons and ions in the plasma. When the electric field and magnetic fields are perpendicular, a circling particle will be accelerated by the electric field such that

$$\boldsymbol{v}_d = \frac{c\boldsymbol{E}_0 \times \boldsymbol{B}_0}{B_0^2} \qquad (4)$$

exerted on the positive ions and electrons that constitute the plasma. The drift velocity is independent of both the charge and the mass of the particle, but this drift could result in a spot of the plasma having a greater density than other regions of the plasma.

For all of the experiments, the equivalent 5.33 Pa and 1.33 Pa experiments resembled each other. In all of the experiments, the accelerations of the particles were more intense for lower pressure. The regions of intense accelerations also grew from the 5.33 Pa experiments to the 1.33 Pa experiments.

When the camera was oriented parallel to the magnetic dipole axis and the horizontal electric accelerations were measured, seen in Figs. 4 and 5, there was an acceleration to the left directly above the magnet. A bit further to the left, there was an acceleration of approximately equal strength to the right. Between these two regions, the horizontal forces were not as strong. The region where the forces are not as strong corresponds to the same region where there was the brighter plasma glow. As can be seen in Fig. 3, the plasma glow is a location of stable particle levitation. From Figs. 4 and 5, there is horizontal confinement in this region. In Figs. 6 and 7, the vertical acceleration is shown. The same region has a dip where the vertical acceleration upwards is less intense. This dip corresponds to this region where there is the plasma glow as well.

In the 5.33 Pa, parallel orientation experiment, the dip is clear. The accelerations upward become less intense as the center of the magnet is approached from the left. As it is approached from the right, it peaks a bit. However, in the 1.33 Pa experiments, a bubble or cavity region is formed, where the acceleration directly above the center of the magnet is almost enclosed by surrounding greater accelerations.

When the camera axis was oriented to be perpendicular to the magnetic dipole axis, the horizontal accelerations are towards the center of the magnet. Above the center of the magnet, where it is least magnetic and the field lines above are parallel to the magnet, there is a dip where the acceleration is less intense, and even approaches zero. Considering the vertical forces, there is acceleration upwards from the table. In the area directly above the magnet, these upwards accelerations become greater. However, similarly to the horizontal acceleration from this orientation, in the region above, there is a dip in the strength of the vertical acceleration above the center of the magnet. For both the horizontal and vertical accelerations, it is weaker above the magnet. As said earlier, the magnetic field lines are parallel to the surface at this region.

The parallel and perpendicular orientation views share a thin slice of data at the center. Strangely, the vertical accelerations from the two different views were not consistent. They had different upwards accelerations at different points. This discrepancy is not yet solved and requires further investigations.

In all of the experiments, when the horizontal accelerations were considered, both 5.33 Pa and 1.33 Pa, both parallel and perpendicular orientations, there were accelerations off the edge of the table. When experiments were conducted without a magnet, this was also the case. This implies that these forces off the table are not caused by the magnet, but rather, the dielectric glass table, itself.

V. Conclusion and Future Works

The experiments that were conducted for this paper are not entirely comparable to a lunar swirl environment. The ratio of Larmor radii and magnetosphere size is roughly the same for experiment and moon. However the requirement for a free molecular flow is not given due to collisions with the neutral gas background. To achieve this requirement the pressure has to be dropped by roughly one order of magnitude. In the current set up, the neutral particle background is too dense, leading to too many collisions of ions and electrons with neutrals. In the GEC RF cell, the plasma routinely shut off at 0.4 Pa. Even with the pressure this low, it was difficult to conduct experiments due to the strong upward forces from the setup. In the future, experiments at even lower pressures should be conducted with heavier particles.

These experiments showed that in a plasma, a weak magnetic field can generate significant horizontal electric forces. These forces can influence dust transport, causing dust to be deposited in specific regions and pushed away from others. In our experiments, we saw that the dust was even transported to regions that the plasma preferred. In these regions, the particles were able to levitate stably, showing strong electric confinement.

These horizontal electric forces can also redirect the solar wind flux, which could cause regions of the Moon to be less exposed to the solar wind, and therefore, be less aged than the surrounding lunar regolith.

These experiments serve as precursor to future experiments and assist in directing future works. Still, they investigated some phenomena and found a stable levitation region within a bright plasma spot. Additionally, both the horizontal and vertical acceleration forces were plotted for two different orientations with the magnet.

ACKNOWLEDGMENTS

Hannah Sabo would like to extend gratitude to the National Science Foundation for funding this research [grant no. 1262031]. Additionally she would like to thank Baylor University and the Center for Atmospheric, Space Physics, and Engineering Research (especially the Space Sciences Lab) for the opportunity to do research this summer. Especially Dr. Truell Hyde and Dr. Lorin Matthews for their guidance throughout the summer. She also thanks Jimmy Schmoke, Mike Cook, and Jorge Carmona-Reyes for laboratory and equipment setup.

REFERENCES

[1] U. Wiechert, A. N. Halliday, D.-C. Lee, G. A. Snyder, L. A. Taylor, and D. Rumble, "Oxygen Isotopes and the Moon-Forming Giant Impact," *Science*, vol. 294, no. 5541, pp. 345–348, Oct. 2001.

[2] J. Zhang, N. Dauphas, A. M. Davis, I. Leya, and A. Fedkin, "The proto-Earth as a significant source of lunar material," *Nat. Geosci.*, vol. 5, no. 4, pp. 251–255, Apr. 2012.

[3] R. A. Bamford, B. Kellett, W. J. Bradford, C. Norberg, A. Thornton, K. J. Gibson, I. A. Crawford, L. Silva, L. Gargate, and R. Bingham, "Mini-magnetospheres above the lunar surface and the formation of lunar swirls," *ArXiv12072076 Astro-Ph Physicsphysics*, Jul. 2012.

[4] J. S. Halekas, D. L. Mitchell, R. P. Lin, S. Frey, L. L. Hood, M. H. Acuña, and A. B. Binder, "Mapping of crustal magnetic anomalies on the lunar near side by the Lunar Prospector electron reflectometer," *J. Geophys. Res. Planets*, vol. 106, no. E11, pp. 27841–27852, Nov. 2001.

[5] X. Wang, C. T. Howes, M. Horányi, and S. Robertson, "Electric potentials in magnetic dipole fields normal and oblique to a surface in plasma: Understanding the solar wind interaction with lunar magnetic anomalies," *Geophys. Res. Lett.*, vol. 40, no. 9, pp. 1686–1690, May 2013.

[6] X. Wang, M. Horányi, and S. Robertson, "Characteristics of a plasma sheath in a magnetic dipole field: Implications to the solar wind interaction with the lunar magnetic anomalies," *J. Geophys. Res. Space Phys.*, vol. 117, no. A6, p. A06226, Jun. 2012.

[7] V. E. Fortov, A. G. Khrapak, S. A. Khrapak, V. I. Molotkov, and O. F. Petrov, "Dusty plasmas," *Phys.-Uspekhi*, vol. 47, no. 5, pp. 447–492, May 2004.

[8] P. J. Hargis, K. E. Greenberg, P. A. Miller, J. B. Gerardo, J. R. Torczynski, M. E. Riley, G. A. Hebner, J. R. Roberts, J. K. Olthoff, J. R. Whetstone, R. J. Van Brunt, M. A. Sobolewski, H. M. Anderson, M. P. Splichal, J. L. Mock, P. Bletzinger, A. Garscadden, R. A. Gottscho, G. Selwyn, M. Dalvie, J. E. Heidenreich, J. W. Butterbaugh, M. L. Brake, M. L. Passow, J. Pender, A. Lujan, M. E. Elta, D. B. Graves, H. H. Sawin, M. J. Kushner, J. T. Verdeyen, R. Horwath, and T. R. Turner, "The Gaseous Electronics Conference radio-frequency reference cell: A defined parallel-plate radio-frequency system for experimental and theoretical studies of plasma-processing discharges," *Rev. Sci. Instrum.*, vol. 65, no. 1, p. 140, 1994.